Applied Surface Science 581 (2022) 152350

Contents lists available at ScienceDirect

Applied Surface Science

journal homepage: www.elsevier.com/locate/apsusc

Full Length Article

Promotion of biofilm production via atmospheric-pressure plasma-polymerization for biomedical applications

Elisa Sainz-García [a,1], María López [b,1], Rodolfo Múgica-Vidal [a,*], Beatriz Rojo-Bezares [b], Carmen Lozano [b,2], Ana González-Marcos [a], Paula Toledano [b], Ignacio Muro-Fraguas [a], Ana Sainz-García [a], Yolanda Sáenz [b,3], Fernando Alba-Elías [a,3]

[a] Department of Mechanical Engineering, University of La Rioja, c/ San José de Calasanz 31, 26004 Logroño, La Rioja, Spain
[b] Molecular Microbiology Area, Center for Biomedical Research of La Rioja (CIBIR), c/ Piqueras 98, 26006 Logroño, La Rioja, Spain

ARTICLE INFO

Keywords:
Atmospheric pressure
Plasma-polymerization
Biofilm
Roughness
Aminopropyltriethoxysilane

ABSTRACT

The ability of bacteria to form biofilms that enhance their resistance to disinfectants and antibiotics is a matter of concern in the fields of food processing and healthcare. Since culture conditions in laboratories are not exactly the same as in the real environments where bacterial infection takes place, developing models that rapidly produce biofilm on test surfaces has become an interesting topic of research. In this work, *Pseudomonas aeruginosa* biofilm production on polystyrene Petri dishes was promoted by atmospheric-pressure plasma-polymerization of 3-(Aminopropyl)triethoxysilane (APTES). Different coatings were deposited varying only the number of plasma-polymerization passes. Biofilm productions, ranging from 157% to 457% relative to that on the uncoated dishes, were quantified after 24-h incubation. According to morphological and chemical characterizations, the APTES precursor promoted biofilm production in several ways: providing amines that facilitated the attachment of more bacterial cells than on uncoated dishes, inducing an oxidative stress to the attached bacteria that caused an overproduction of extracellular polymeric substances, and generating siloxane-based particles that formed a granular pattern that facilitated bacterial accumulation in its valleys. Comparing the coatings, a direct relationship was identified between the number of plasma-polymerization passes, the roughness and the biofilm production.

1. Introduction

Bacterial populations inhabit innumerable environments, and their growth in surfaces is mostly associated with biofilm formation [1]. The biofilm is a complex aggregate of bacteria encased in a self-generated matrix of extracellular polymeric substances (EPS), and is one of the key strategies for the survival of species during unexpected changes of living conditions such as temperature fluctuation and nutrient availability. Proper elimination of biofilms from, for example, food-contact surfaces, processing equipment, medical devices and implants plays a vital role in guaranteeing an optimal microbiological state of quality [2–5]. In fact, it is known that the bacteria of clinical relevance —such as *Pseudomonas aeruginosa*, *Staphylococcus aureus*, and *Acinetobacter baumannii,* among others— encased in a biofilm are up to 1,000 times more resistant to host defense mechanisms and antibiotics when compared to planktonic cells [6,7]. Biofilms account for 80% of chronic microbial human infections, leading to increased rates of hospitalization, elevated health care costs, and increased mortality and morbidity rates [5]. Therefore, significant efforts are being made to design novel antibiofilm surfaces in food industry and medicine [8–12]. More specifically, *P. aeruginosa* is a common Gram-negative and notoriously resistant bacterium, able to adapt and survive in unfavorable environmental conditions which can cause a wide range of illnesses and food spoilage [13]. The great impact of *P. aeruginosa* infection is mainly due to its

* Corresponding author.
E-mail addresses: elisa.sainzg@unirioja.es (E. Sainz-García), mlopezm@riojasalud.es (M. López), rodolfo.mugica@unirioja.es (R. Múgica-Vidal), brojo@riojasalud.es (B. Rojo-Bezares), carmen.lozano@unirioja.es (C. Lozano), ana.gonzalez@unirioja.es (A. González-Marcos), ptoledano@riojasalud.es (P. Toledano), ignacio.muro@unirioja.es (I. Muro-Fraguas), ana.sainz@unirioja.es (A. Sainz-García), ysaenz@riojasalud.es (Y. Sáenz), fernando.alba@unirioja.es (F. Alba-Elías).
[1] These authors contributed equally to this work.
[2] Present address: Area of Biochemistry and Molecular Biology, University of La Rioja, c/ Madre de Dios 51, 26006 Logroño, La Rioja, Spain
[3] These senior authors contributed equally to this work.

https://doi.org/10.1016/j.apsusc.2021.152350
Received 8 October 2021; Received in revised form 10 December 2021; Accepted 24 December 2021
Available online 1 January 2022

capability to form biofilm [14]. *P. aeruginosa* also effectively colonizes a variety of surfaces including medical materials (urinary catheters, implants, contact lenses, etc.) [12], and food industry equipment (mixing tanks, vats and tubing) [15]. *P. aeruginosa* is a well-known biofilm former, which makes it an excellent model to study biofilm formation and has been used during the last years in many studies aiming at the prevention of bacterial adhesion and biofilm formation [16–18]. Furthermore, biofilms are commonly used in the water treatment technology. There is an increasing need for application of biofilm process in the upcycling of wastewater treatment plants all around the world in recent years. They are formed on the fixed media whether it is sand, gravel, plastic or activated carbon. They are part of the water treatment units such as the trickling filters, single pass filters, recirculating filters, rotating biological contactors, and submerged filters [19]. Food industry is another field in which biofilms is used to produce fermented food as cheese, pickle, among others.

However, there are other fields, such as in clinical microbiology, biotechnology or basic research where the overproduction of biofilm can be an advantage. The main objectives in clinical microbiology are the identification of the pathogen that causes an infection and the analysis of the antimicrobial susceptibility of this pathogen, determining the best antibiotic to combat the agent and the optimal antimicrobial dose to be used. However, the classic antimicrobial susceptibility tests (from disk diffusion to automatic broth microdilution methods) that provide the minimal inhibitory concentration (MIC) used to define the susceptibility breakpoints and the PK/PD parameters to predict therapeutic success, as well as the current antimicrobial susceptibility testing methods used in routine clinical practice are based on the study of bacteria in planktonic state. This approach is not adequate to determine the antimicrobial phenotype of bacteria growing in biofilms, and subsequently is not adequate to determine the correct treatment. Thus, the lack of correlation between conventional susceptibility test results and therapeutic success in chronic infections is probably a consequence of the use of planktonic-growing instead of biofilm-growing bacteria [20,21].

On the other hand, in the laboratory the generation of a mature biofilm usually takes at least 24–72 h, and then, antimicrobial phenotype would be determined. However, patient's care demands fast susceptibility testing against infectious diseases. Hence, new analytical methods should surmount challenges on different aspects such as sensitivity (avoiding tedious bacterial cultures and contamination chances), accuracy, reproducibility, fastness, simplicity, cost-effectiveness, multiplexing capabilities and portability possibilities, among others.

Since 80% of the bacterial infections are produced by bacteria in biofilm form [5], it is desirable that the studied pathogenic microorganism in the laboratory produces as much biofilm as it would produce in a patient in a short period of time. For all the aforementioned, with the objective of facilitating drug and disinfectant testing against biofilms of *P. aeruginosa* and other bacterial species, several recent works have been carried out to develop *in vitro* [20,22–24] and *ex vivo* models [25] that rapidly mimic biofilm formation in patients (i.e., *in vivo*) and on surfaces of healthcare facilities.

The use of atmospheric-pressure plasma for biomedical and food applications has been explored in various ways in the last few years and have shown promising effects such as bactericidal, antifouling or biocompatibility [4,26–32]. In fact, this technology is considered one of the most promising approaches to tune surface properties via coating deposition for several reasons: (a) it is able to modify thin surface layers of conventional materials with no alteration of the bulk, (b) it produces continuous, homogeneous, and pinhole-free coatings, (c) it is a dry technology with no use of solvents (gas-phase dry processes), (d) it makes a reduced and effective use of chemicals that promotes economic and environmental benefits, (e) it has great versatility, being applicable to a broad range of substrates and complex-shaped structures, facilitating the development of universal polymer coatings, and (f) its integration in industrial processes is relatively easy [33–36]. Nevertheless, to the best of our knowledge, the use of atmospheric-pressure plasma to promote biofilm production on surfaces for laboratory studies remains unexplored.

Considering the interest that has recently aroused in the development of models for rapid biofilm formation, this paper aims to promote the production of bacterial biofilm through the plasma-polymerization of (3-aminopropyl)triethoxysilane (APTES) coatings produced by an atmospheric-pressure plasma system on polystyrene (PS) Petri dishes. APTES is used as the precursor because, as we observed in previous works, it can produce plasma-polymerized coatings that are stable in humid environment [37]. Different numbers of plasma-polymerization passes will be used in order to identify the process conditions that promote the pro-biofilm characteristics of the coatings. The coatings obtained will be subjected to morphological and chemical characterization, as well as to measurements of their water contact angle (WCA). Biofilm production during 24-h incubation will be quantified using *P. aeruginosa* PAO1 strain as the reference microorganism, and the mechanism by which biofilm is produced on the coated Petri dishes will be discussed.

2. Experimental

2.1. Materials

The silane (3-Aminopropyl)triethoxysilane (APTES; $(CH_3CH_2O)_3$-Si-$CH_2CH_2CH_2NH_2$, Sigma–Aldrich) was the liquid precursor used in this work. PS Petri dishes (in advance, samples) with a diameter of 30 mm were used as substrates. The samples that have been used in this study were previously plasma-treated by their manufacturer (Thermo Scientific™ Nunc™ Cell Culture/Petri Dishes) for surface activation.

2.2. Plasma-polymerization process

The samples were coated by a plasma-polymerization process with a rotational pattern by the Atmospheric Pressure Plasma Jet (APPJ) system of the University of La Rioja (PlasmaSpot500® purchased from MPG, Luxembourg). This APPJ system (Fig. 1) has two coaxial electrodes and the plasma is generated from a gas that flows between them. The internal electrode is grounded and the external one is excited with a 68 kHz frequency by a high voltage source. The atomized precursor is introduced through the internal electrode until it arrives to the action zone of the plasma. Then, the precursor is transformed by the reactions that take place in the gas phase of the plasma. The parameters that were

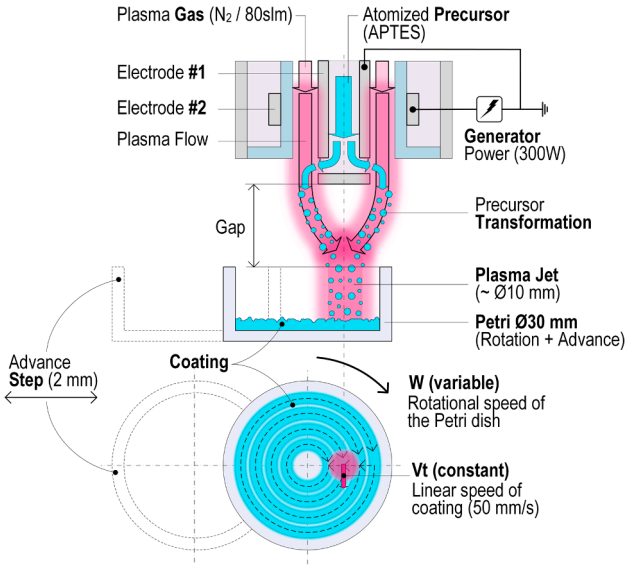

Fig. 1. Scheme of the plasma-polymerization process with a rotational pattern.

used in the plasma-polymerization process are shown in Table 1. The process had two stages. In the first stage, the sample was treated with 4 passes of the plasma generated from nitrogen to clean and activate its surface. In the second stage, the sample was coated with several passes adding APTES to the plasma, according to the specifications in Table 2. A "pass" is defined as each time that the plasma jet travels over the whole base of the Petri dish. The rotational pattern of movement that was used during the process was designed in a way that the whole surface of the sample was homogeneously coated by maintaining a constant linear speed (50 mm/s). A scheme of the plasma-polymerization process is shown in Fig. 1, which includes a representation of the rotational pattern. With these linear speed and rotational pattern, each pass was performed in 8.3 s.

2.3. Morphological characterization

The surface morphology of the studied samples was analyzed by Atomic Force Microscopy (AFM) in tapping mode using a Multimode AFM (Bruker Corporation) atomic force microscope with a Nanoscope V controller. The analyzed images were obtained by scanning 40 × 40 μm areas. The arithmetic average roughness (Ra) values for each sample were calculated as the average of three different measurements per sample by means of NanoScope Analysis 1.4 software. Furthermore, the distance between peaks was obtained from the AFM data. First, 2D profiles were extracted from the 3D AFM images. In order to prevent the detection of false peaks, the signal distortion was attenuated through profile smoothening. Then, the amplitude of the peaks was compared to a threshold to exclude very small peaks and detect the major peaks. Finally, the positions of these peaks in the profiles were determined and the distance between consecutive peaks was averaged.

A Scanning Electron Microscope (SEM) HITACHI S-2400 operating at 18 kV was used to examine the surfaces of the coated and uncoated samples. The samples were made conductive by plasma gold–palladium sputtering before SEM examinations to prevent charging.

2.4. Chemical characterization

Attenuated Total Reflectance-Fourier Transform Infrared Spectroscopy (ATR-FTIR) by means of a Perkin Elmer Spectrum Two FTIR spectrometer was used to investigate the chemical composition of the coated samples. The spectra were collected in the transmission mode using 32 scans per spectrum at a resolution of 4 cm^{-1}. The data were analyzed using the Spectrum software (version 10.4.3.339); automatic base line correction was applied to all spectra.

The surface chemistry of the samples was determined using an X-ray Photoelectron spectrometer (XPS-AES) Kratos AXIS Supra (Kratos Analytical) with a multi-channel hemispherical analyzer to quantify the relative atomic percentages of the elements at the coatings and the uncoated PS. The samples were irradiated with a monochromatic AlKα X-ray source (225 W, 15 kV, 1486.69 eV). The spectra were acquired at a constant pass energy of 160 eV (general spectra) and 20 eV (high-resolution spectra) using the Kratos ESCApe software. Chemical constituents were identified using the observed peak positions in the measured spectra [38]. Results were obtained from three different measurement locations on each sample surface. Spectra post-processing was done using Casa XPS software (version 2.3.16, Casa Software Ltd.). All spectra were charge-corrected by adding 4.3 eV to give the adventitious C 1s component a binding energy of 285 eV. Finally, the C 1s signal of the XPS spectra of some of the samples were deconvoluted by means of PeakFit 4.12 (SPSS Inc.) software.

Table 1
Parameters of the plasma-polymerization process.

Parameter	
Plasma gas	Nitrogen (99.999%)
Plasma gas flow (slm)	80
Plasma power (W)	300
Precursor	APTES
Precursor carrier gas	Nitrogen (99.999%)
Precursor gas flow (slm)	1.5
Step (mm)	2
Lineal speed (mm/s)	50

Table 2
Codification of samples according to the number of plasma-polymerization passes.

Sample	Passes
S0p	0
S4p	4
S8p	8
S12p	12
S24p	24
S48p	48
S72p	72
S96p	96

2.5. Wettability measurements

The wettability of the studied samples was assessed through static water contact angle (WCA) measurements by the sessile drop method. 10 μL water droplets were placed on the samples' surface and the WCA was determined by image analysis using the software ImageJ [39] with the plugin for low-bond axisymmetric drop shape analysis [40]. For each sample, the WCA was calculated as an average of three measurements. Furthermore, the work of adhesion (W_{adh}) between water and the studied samples was calculated using the formula

$$W_{adh} = \gamma_{lv}{}^{*}(1 + \cos\theta)$$

where γ_{lv} is the surface tension of water (72.8 mJ/m^2) and θ is the WCA [41].

2.6. Bacterial strain and growth conditions

The reference *P. aeruginosa* PAO1 strain was obtained from type culture collection. It was routinely cultivated in Brain Heart Infusion Agar (CondaLab, Spain) and incubated for 24 h at 37 °C.

2.7. Biofilm quantification and bacterial growth

The capacity of bacteria to form biofilm in uncoated and coated samples was evaluated. For this purpose, an initial 10^6 cfu/mL inoculum of P. aeruginosa PAO1 in Müeller Hinton broth (CondaLab, Spain) was added to Petri dishes (PS 30 mm) using 3 ml per sample. Plates were incubated for 24 h at 37 °C to obtain a mature biofilm.

For the quantification of biofilm, Fluorescein Diacetate (FDA) method was used. Non-specific intra and extracellular esterases of viable microbial cells are capable of converting non-colored, non-fluorescent fluorescein diacetate (FDA) into yellow, highly fluorescent fluorescein. FDA (Sigma) has been used for measuring total microbial activity in different substrates, as well as for the quantification of biofilm biomass [42]. In this way, after 24 h of biofilm formation, the supernatant was removed, and the plates were rinsed with 3 ml of 100 mM MOPS buffer (pH7, MOPS, Sigma). FDA was dissolved in acetone in a concentration of 10 mg/ml, and this stock solution was stored at − 20 °C. Starting from the stock solution, a 1:100 FDA working solution in MOPS buffer was freshly prepared before each assay. Then, 3 ml of FDA working solution was added to each sample that were incubated 1 h at 37 °C in a dark atmosphere. After this time, fluorescent measures using an excitation/emission wavelength of 494/518 nm were performed using a POLARstar Omega microplate reader (BMG Labtech) [20]. All the assays were performed in triplicate.

For each sample tested, the relative biofilm production (%) was calculated as follows:

Relative biofilm production = $\left(\text{Fluorescence}_{\text{coated sample}}/\text{Fluorescence}_{\text{uncoated sample}}\right)*100$

Values of relative biofilm production lower than 100% indicate a potential anti-biofilm activity and values higher than 100% indicate a potential pro-biofilm activity of the tested coatings.

In addition, the bacterial growth of each sample was determined measuring the absorbance at 620 nm using a Microplate Reader 680XR Bio-Rad photometer after 0, 3, 6 and 24 h of incubation of 10^6 cfu/mL *P. aeruginosa* PAO1 inoculum in Müeller Hinton broth.

2.8. Biofilm visualization through SEM

The biofilm that was produced on coated and uncoated samples after 24-h incubation was examined by SEM. After incubation, the samples were washed twice with Ringer buffer. Biofilm fixation was done applying 2.5% glutaraldehyde phosphate buffered saline (TAAB Laboratories, UK) at 4 °C for 2 h, followed by three times washing with phosphate buffered saline (PBS, Sigma). Then, the samples were treated for 2 h with 2% osmium tetroxide PBS (TAAB laboratories, UK). Afterwards, they were washed three times with PBS and dehydrated with ethanol (Panreac) in increasing concentrations: 30% (30 min), 50% (30 min), 70% (30 min), 90% (30 min), 3 × 96% (30 min) and 3 × 100% (30 min). Then, the samples were dried by a CDP 030 critical point dryer (BAL-TEC Inc., Liechtenstein) and gold-coated by a SCD 004 sputter coater (BALZERS, Liechtenstein). Finally, the samples were observed using a JEOL JSM-6480 LV scanning electron microscope (JEOL, Japan).

3. Results and discussion

3.1. Morphological characterization

The surface morphology of the uncoated PS substrate (sample S0p) and coated samples was studied through AFM and SEM. Fig. 2 depicts the average roughness of all samples. Fig. 3 illustrates SEM images, whereas Fig. 4 shows AFM images of all samples. Fig. 5 shows the AFM profiles of samples S4p, S8p, S12p and S72p.

Fig. 2 shows that the roughness increased as the number of passes increased. SEM and AFM images of the uncoated PS substrate (Fig. 3[a] and 4[a]) exhibited a smooth appearance, although it was also possible to observe numerous marks and particles of the PS substrate (Fig. 3[a]). As successive passes were applied, the surface of the coated samples (Fig. 3[b]-[h] and 4[b]-[h]) changed from being practically smooth (S4p) to showing a granular structure with peaks and valleys (S96p) that is typical of silicon oxide-based coatings [43,44]. As observed in other works in which APTES-based coatings have been applied [44], the marks and particles of the PS substrate seem to have acted as nucleation sites from which the granular structure of the coatings was formed. An increase in the number of passes implies prolonging the treatment time, which favors precursor fragmentation and recombination of different particles during the plasma-polymerization process [45]. This finally causes an increase in the size of the granules that form the coating. This granular growth is also a consequence of the geometric interaction between the angular direction of the coating species that arrive to the surface under treatment and the topography of the growing film, which causes a shadowing effect. This makes the deposition rate of the coating species to be higher at the top of the surface features (i.e., marks and particles), where they have a wider incident angle for arrival than at the valleys between those features [46,47]. As a result of this growth mechanism, there was an increase in roughness (S4p: 16.5 nm → S96p: 105 nm).

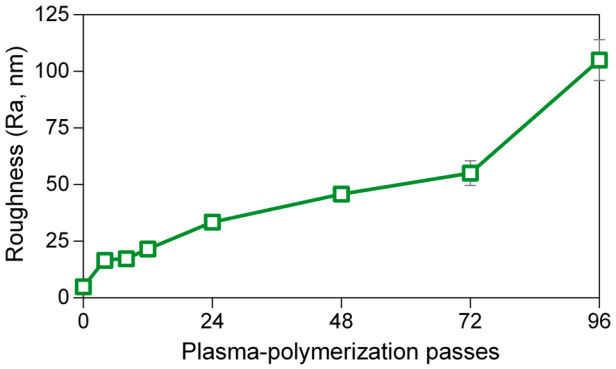

Fig. 2. Average roughness (Ra) of all the analyzed samples.

Comparing the AFM profiles of the coatings shown in Fig. 5, it can be confirmed that the size of the granules increased as the number of passes increased. For each AFM profile, a scheme of the growth of the coating and the average distance between its granules were included. This distance increased as the size of the granules increased. As indicated in Section 3.5.1. *Effect of coating morphology*, the size and distance between the granules that form the coating can explain the observed tendency in the biofilm production in this work.

3.2. Attenuated total Reflectance-Fourier Transform Infrared (ATR-FTIR) Spectroscopy

ATR-FTIR analysis was conducted to chemically characterize the coated samples. The peaks in the IR spectra of Fig. 6 were used to confirm the different functional groups present in the APTES molecule. As it was confirmed in a previous work [44] that used the same plasma-polymerization system and precursor, three main regions can be identified. In Region A (960–1260 cm^{-1}), a broad band can be observed that corresponds to the overlapping of SiOSi, SiOC and OCH_2CH_3 functional groups. In Region B (1500–1800 cm^{-1}), peaks related to amines, amides, imines and C = O are identified. Finally, the wide adsorption band around 3000–3700 cm^{-1} (Region C) is due to the OH and NH functional groups. In addition to the abovementioned, other overlapped peaks could be identified that belong to the plasma treated polystyrene's ATR-FTIR spectrum: C-O stretching at ~ 950 cm^{-1}, C = C stretching and C = O groups around 1600 cm^{-1} and hydroxyl groups at ~ 3650 cm^{-1}. The remaining observed peaks corresponded to the ATR-FTIR spectrum of PS, as other authors have identified [48]: C-H out of phase bending at ~ 695 cm^{-1}, CH_2 bending at ~ 1320 cm^{-1}, and stretching of aliphatic and aromatic C-H in the range 2800–3000 cm^{-1}.

It is worth noting that the detected functional groups were the same for all the coated samples. Nevertheless, a variation in the intensity of the spectra was observed, and related to the number of passes that were applied to coat the samples (Fig. 6). The higher the number of passes, the higher the intensity of the ATR-FTIR spectrum was. As other authors explained, the relative thickness of a coating can be quantified from the area under an ATR-FTIR peak that is associated with a chemical bond that is unique of a coating and not present in the substrate [49]. Therefore, although the coating thickness was not measured in this work, the observed variation in the intensity of the ATR-FTIR spectra, which was particularly remarkable at the wavenumbers of the bonds of silicon from APTES (Region A), seems to be a clear sign of the variation in the coating thickness according to the number of passes. The higher the number of passes, the higher the intensity of the ATR-FTIR spectrum and the area below it and, therefore, the higher the thickness of the plasma-polymerized coating was. Considering these results, it can be inferred that increasing the number of passes caused an increase in the coating thickness, while the chemical composition remained similar for all the coated samples.

3.3. X-ray Photoelectron Spectroscopy (XPS)

XPS analysis was carried out to determine the atomic chemical composition of the samples within the first 3–5 nm in depth. Table 3 shows the atomic percentage of the chemical elements for each analyzed

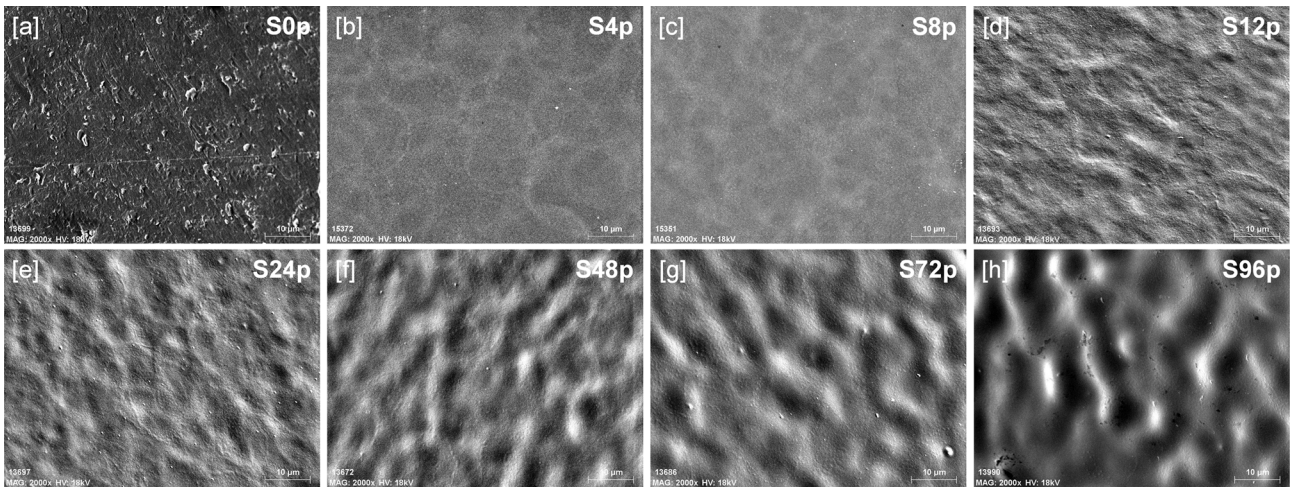

Fig. 3. SEM images (x2000) of all the analyzed samples.

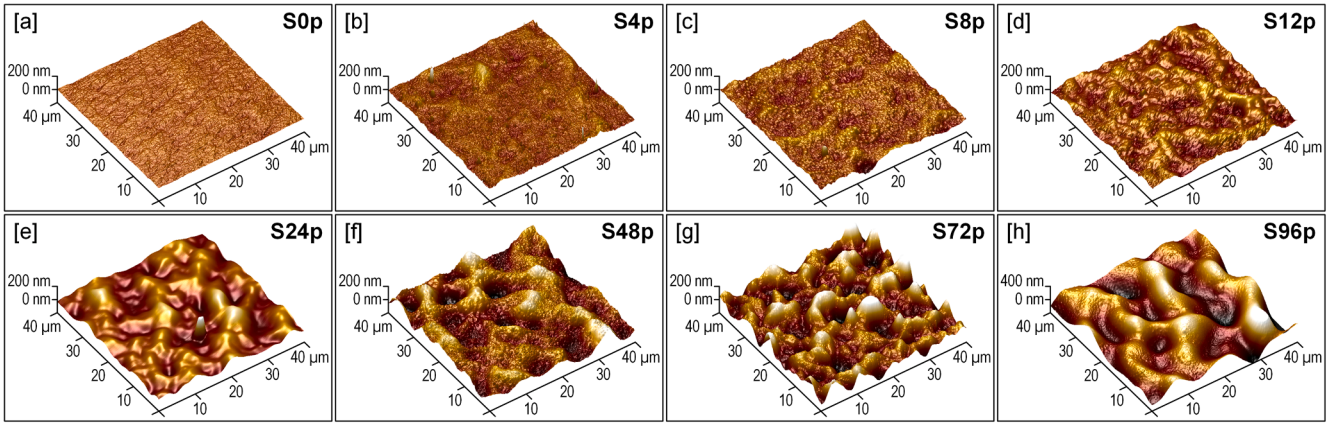

Fig. 4. AFM images (40x40μm) of all the analyzed samples.

sample. The uncoated sample (S0p) contained carbon (C), oxygen (O) and nitrogen (N), and the coated samples harbored silicon (Si), in addition to the foregoing elements. The presence of these elements (C, O, N and Si) in the coated samples comes from the plasma-polymerization of APTES and from the surrounding air of the coating process.

Regarding the uncoated sample (S0p), its atomic percentages of C, O and N were similar to those associated with plasma treated polystyrene [28,48,50], and significantly different from those of the coated samples. Regarding the coated samples, it is worth noting that APTES layers were quite homogeneous. The percentages of the identified elements were similar among them and quite similar to those previously computed by these authors in other works using both the same precursor (APTES) and the same deposition technology (APPJ) on other polymeric substrates [37,44,51]. So, no significant difference was observed among samples. This means that, although the thicknesses of the coatings were different, the layers that were deposited in successive passes did not provoke chemical alterations to each other.

Since no significant differences were found among the elemental compositions of the different coated samples, the deconvolution of C 1s high-resolution spectra of samples S0p, S4p and S72p was carried out to analyze their surface chemistry more thoroughly. Fig. 7 shows these deconvolutions, and Table 4 the corresponding peak positions of the functional groups in the C 1s spectra.

The deconvolution of the uncoated sample (S0p, Fig. 7[a]) showed the functional groups that are typically associated to carbon in a plasma-treated PS surface: [A] C-C and C-H (aromatic rings), [B] C-C y C-H (aliphatic carbons), [C] C-O/C-N groups, [D] O-C = O groups and [E] π-π^* component [50]. Groups [A], [B], [C] and [E] come from the PS molecule. The presence of C-O (~286.5 eV) can be attributed to either additives in the polymer or partial oxidation of the PS surface, and the π-π^* component is characteristic of aromatic rings of the PS macromolecule [50]. On the other hand, the plasma treatment that was applied by the manufacturer to the PS Petri dishes exhibited the following groups: [C] C-N bonds at ~ 286.5 eV and [D] O-C = O groups at ~ 289.5 eV characteristic of carboxylic acids. When the PS Petri dishes were coated by plasma-polymerization of APTES, groups [A], [D] and [E] disappeared, and groups of [F] C-Si and [G] C = O that come from the polymerized APTES appeared [52,53]. Finally, groups [B] and [C] were common of both the plasma-activated PS and the plasma-polymerized APTES (Fig. 7 [b],[c]), as it was also previously reported [52,53]. Oxygenated carbon groups (i.e., C-O, O-C = O and C = O) have been reported to cause oxidative stress to cells in contact with them [54]. Therefore, their presence in the C 1s region of the analyzed samples was quantified as the percentage of the area under each XPS spectrum that corresponded to the sum of the areas of peaks [C], [D] and [G]. A more prominent presence of oxygenated carbon groups was detected in the coated samples S4p (40.4% ± 1.8) and s72p (44.2% ± 0.7) than in the uncoated sample (24.5% ± 3.1).

The analysis of the atomic percentages and chemical groups could conclude that the surface chemical structures of the coated samples (S4p and S72p) and of the uncoated sample (S0p) were very different due to both their elemental composition (atomic percentages of C, O, Si and N in Table 3) and the bonds associated to carbon (Fig. 7). The chemical structures of the coated samples S4p and S72p, which are representative

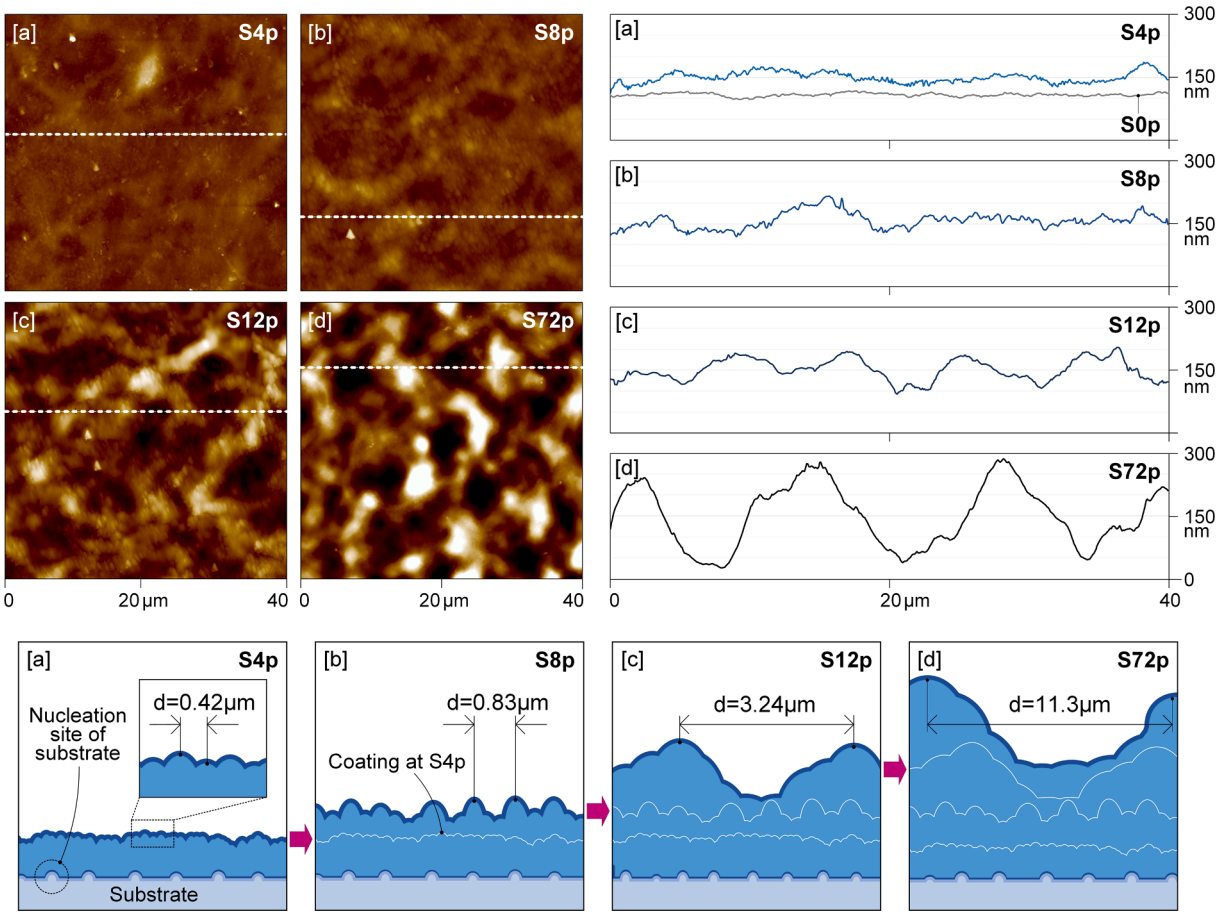

Fig. 5. AFM images, 2D profiles along the dashed lines and coating growth schemes of samples [a] S4p, [b] S8p, [c] S12p and [d] S72p.

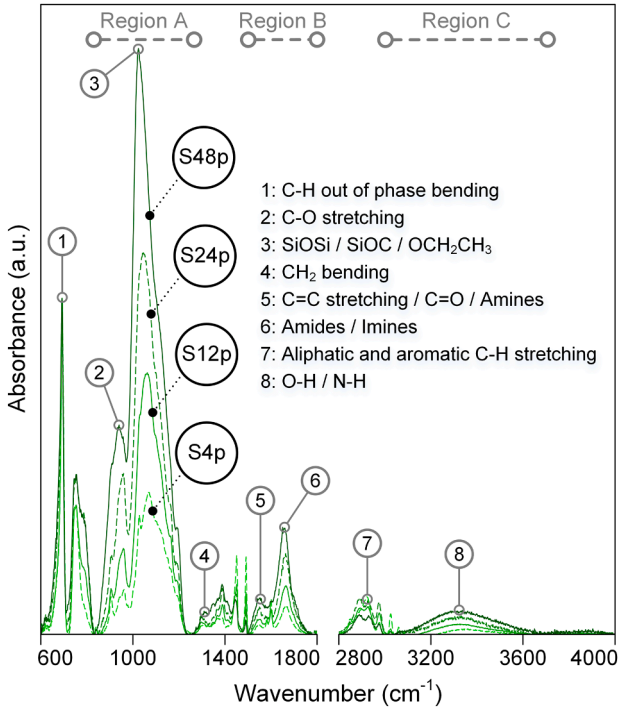

Fig. 6. ATR-FTIR spectra of samples S4p, S12p, S24p and S48p.

Table 3
Atomic percentages of C, O, N and Si of all the analyzed samples.

Sample	Elemental composition (at. %)			
	C1s	O1s	N1s	Si2p
S0p	83.00 ± 1.23	13.17 ± 0.76	2.96 ± 0.48	0.77 ± 0.17
S4p	48.10 ± 0.81	34.88 ± 0.82	4.97 ± 0.15	12.05 ± 0.31
S8p	48.68 ± 1.09	34.06 ± 1.03	5.09 ± 0.22	12.17 ± 0.14
S12p	49.63 ± 2.28	33.13 ± 1.84	5.10 ± 0.26	12.14 ± 0.90
S24p	49.19 ± 0.92	33.72 ± 1.04	5.30 ± 0.59	11.79 ± 0.42
S48p	50.53 ± 3.49	31.99 ± 3.46	4.81 ± 0.35	12.39 ± 0.09
S72p	48.87 ± 1.16	33.80 ± 1.68	4.92 ± 0.31	12.51 ± 0.98
S96p	51.01 ± 1.53	32.39 ± 1.07	4.80 ± 0.12	11.80 ± 0.59

of all the samples that were coated with APTES in this work, were very similar to each other regardless the considerable difference in their roughness (Ra values of 16.50 nm and 55.10 nm, respectively, in Fig. 2 and Table 5).

3.4. Wettability

When a solid surface is exposed to a liquid, an angle is formed between the liquid–vapor interface and the solid surface where they meet. This is known as the contact angle, whose value depends mainly on the relationship between the liquid–solid adhesive forces and the cohesive forces of the liquid. Surfaces with higher WCA have lower droplet adhesive forces [55]. According to the literature, the wettability of a surface is one of the factors influencing its interaction with bacterial cells. It is considered that hydrophobic (WCA > 90°) and superhydrophobic (WCA > 150°) characters favor the achievement of antibacterial effects

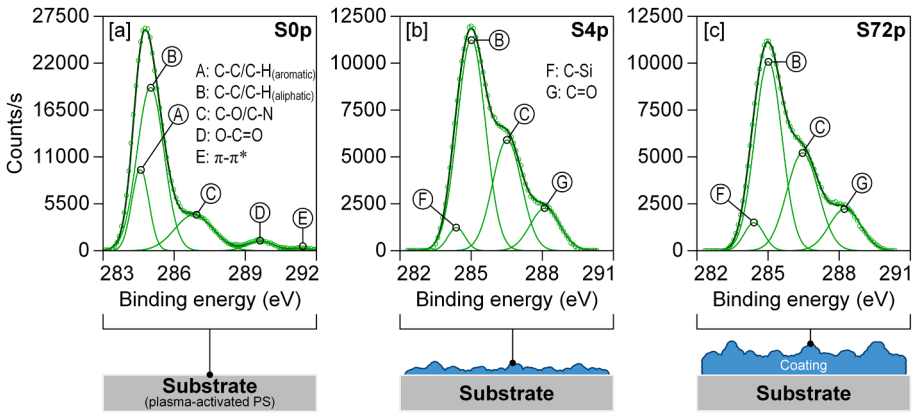

Fig. 7. High-resolution C 1s spectra of samples [a] S0p, [b] S4p and [c] S72p.

Table 4
Binding energies and functional groups of C 1s deconvolutions.

	Functional groups	Peak position (eV)	References
A	C-C/C-H *aromatic rings*	~284.6	[50]
B	C-C/C-H *aliphatic carbons*	~285.0	[50,52,53]
C	C-O/C-N	~286.5	[50,52,53]
D	O-C = O	~289.5	[50]
E	π-π*	~291.3	[50]
F	C-Si	~284.4	[52]
G	C = O	~288.2	[53]

Table 5
Ra, WCA and W_{adh} of all the analyzed samples.

Sample	Roughness (Ra, nm)	WCA (°)	W_{adh} (mJ/m^2)
S0p	4.87 ± 1.13	54.72 ± 2.30	114.85
S4p	16.50 ± 0.28	56.58 ± 0.81	112.79
S8p	17.27 ± 1.83	55.67 ± 1.57	113.86
S12p	21.55 ± 2.19	57.06 ± 1.49	112.39
S24p	33.45 ± 1.34	56.76 ± 2.87	112.71
S48p	45.80 ± 1.56	56.23 ± 1.77	113.27
S72p	55.10 ± 5.44	56.59 ± 2.02	112.89
S96p	105.00 ± 9.00	64.44 ± 3.05	104.21

because they weaken the adhesion of biofilm and bacteria to the surface [33]. The wettability of the analyzed samples was determined by measurements of the static WCA, and the average WCA and W_{adh} of each sample are shown in Table 5. All the studied samples were hydrophilic (WCA < 90°), and in addition, all the coated samples (except S96p) had very similar WCA and W_{adh} values. In the particular case of sample S96p, it seems that although its chemical composition was similar to those of most of the coated samples, its much higher roughness (105 nm) resulted in a higher WCA (64.44°) and a lower W_{adh} (104.21 mJ/m^2) than those of the remaining coated samples.

3.5. Biofilm and bacterial quantification

Total biomass formation in the biofilm was evaluated using FDA method. The amount of biofilm that was generated on the uncoated sample (S0p: 100%) was used as the control for the comparative study of the coated samples. Thus, the coatings that generated an amount of biofilm < 100% are defined as anti-biofilm whereas those that generated an amount of biofilm > 100% are defined as pro-biofilm.

3.5.1. Effect of coating morphology

Fig. 8 shows the relationship between the roughness of the APTES-based coatings and the percentage of biofilm that was produced on their surfaces by *P. aeruginosa* after 24-h incubation. As it is shown in

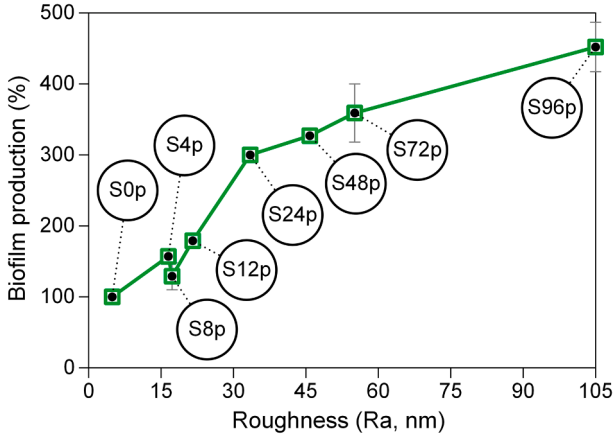

Fig. 8. Relationship between the roughness of the coatings and the biofilm produced (shown as percentage respect to the uncoated PS, S0p, 100% biofilm).

Fig. 8, all the coatings of this work were pro-biofilm (>100%). In addition, a direct relationship between the number of passes, the roughness and the biofilm production can be identified in all samples except S8p. The higher the number of plasma-polymerization passes, the higher the roughness and the biofilm production were. As Fig. 3 and Fig. 4 show, when the number of passes increased, the coating became rougher and changed from a smooth morphology to a granulated structure that is typical of silicon oxide-based coatings.

As other authors identified, while a large surface area with rough topography can promote bacterial adhesion, topographical patterns that are favorable for bacterial adhesion cannot be generalized because the shape and size of bacteria also play roles in bacterial interactions with the surfaces of materials. As schematized in Fig. 9, the spatial distribution of roughening structures and macroscopic/microscopic patterns on surfaces, relative to bacterial size and shape, are important parameters for bacterial adhesion [56–61]. This fact was corroborated by SEM images of the biofilms. In this sense, Fig. 10 shows the SEM images of sessile bacteria on biofilms for samples S0p and S72p. Although the initial amount of bacteria in the inoculum was the same on coated and uncoated samples, a higher accumulation of sessile bacteria seemed to take place in the valleys of the granular pattern of the coating and resulted in a higher biofilm production (S0p: 100%; S72p: 359%). This tendency of bacteria to accumulate in the valleys of surface topography is widely described in the scientific literature [62–64].

Regarding sample S8p, it is of great interest to understand why its behavior was different to the rest of the samples. Fig. 5[a],[b] shows the AFM images, as well as a transversal profile (40 μm) obtained from the AFM image, of samples S4p and S8p. According to the general trend that

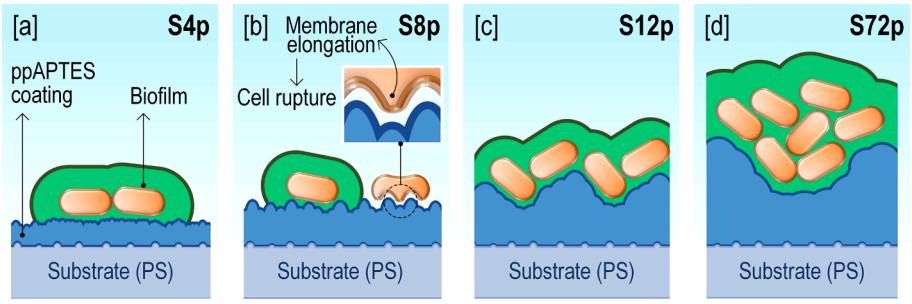

Fig. 9. Behavior of *P. aeruginosa* bacteria according to the surface topographies of the coated samples [a] S4p, [b] S8p, [c] S12p and [d] S72p.

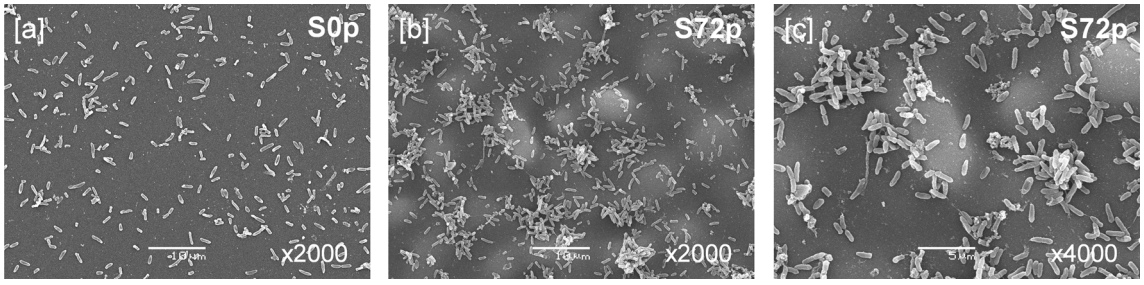

Fig. 10. SEM images of biofilms: [a] sample S0p and [b,c] sample S72p.

was identified in Fig. 8, and considering the fact that the Ra of sample S8p is somewhat higher than that of sample S4p (S4p: 16.50 nm; S8p: 17.27 nm), a similar or higher biofilm percentage could be expected on sample S8p compared with sample S4p. Nevertheless, the biofilm percentage of sample S8p was lower than that of sample S4p (S4p: 157%; S8p: 129%). As Fig. 5[b] shows, the granular pattern of sample S8p had a peak-to-peak distance of 0.83 μm. On the other hand, the size of the bacterial cells is in the range of 2–4 μm [65]. The ratio between that peak-to-peak distance (0.83 μm) and the size of the bacteria (2–4 μm) reduces the contact area between the bacteria and the coating, thus leading to lower bacterial adhesion [62] and even to the elongation of the cell membrane, which may cause bacterial damage and death [66]. This would explain the lower biofilm production of sample S8p, compared with the production of sample S4p.

3.5.2. *Effect of coating chemistry*

Until now, the pro-biofilm behavior of the APTES-based coatings has been explained only as a function of their roughness. Nevertheless, some studies [67] argue that the increase in the biofilm percentage is also due to the modification in the surface chemistry, which causes an increase in the attachment of biofilm-forming microorganisms. The chemical nature of the coatings was analyzed by ATR-FTIR and XPS. The ATR-FTIR spectra of all the coated samples showed the same peaks (Fig. 6), including those associated with amines (NH_2) and siloxanes (SiOSi) from the APTES precursor, and their intensities were proportional to the number of passes. Furthermore, the XPS analysis showed a more prominent contribution of oxygenated carbon groups to the bonds of carbon at the surface of the analyzed samples.

Amine groups have been reported to accept protons from adsorbed water and generate sites with positive charge [68]. Since *P. aeruginosa* bacteria have a negative charge, they could be electrostatically attracted by the positively charged sites of the amine groups (Fig. 11). This fact may have facilitated the attachment of more bacterial cells to the coatings than to the uncoated PS during the first stages of surface colonization (Fig. 11[b]). Furthermore, oxygenated carbon groups induce oxidative stress [54], and it has been previously reported [69,70] that *P. aeruginosa* bacteria overproduce EPS to protect themselves from oxidative stress (Fig. 11[c]). The more prominent presence of oxygenated carbon groups at the surface of the coatings than at the uncoated PS would have induced a higher degree of oxidative stress, thus leading to the overproduction of higher amounts of EPS. Therefore, the differences in the chemistry of the coatings respect to that of the uncoated PS seem to have contributed to the pro-biofilm character of all the coatings.

Comparing the coatings, no significant differences were found in their elemental composition or in the amount of the identified chemical groups that could directly explain their different biofilm productions. Nevertheless, the presence of silicon oxide-based groups in the coatings has been confirmed by their chemical characterization. Indeed, as discussed in Section 3.5.1, the differences in their pro-biofilm behavior have been explained as a function of their roughness, which rises from

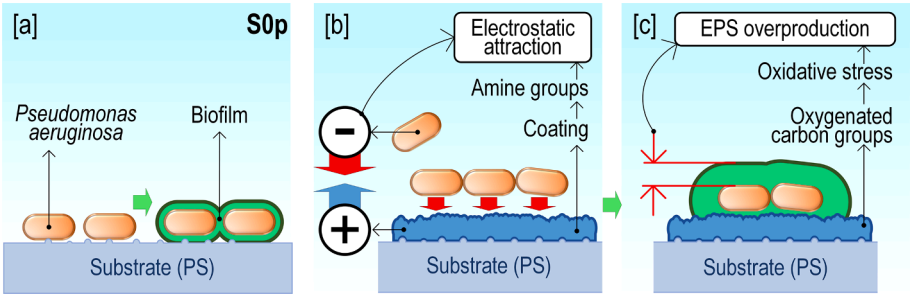

Fig. 11. Scheme of *P. aeruginosa* biofilm formation on [a] the uncoated sample and [b,c] the coated samples.

the accumulation of silicon oxide particles coming from the APTES precursor as successive plasma-polymerization passes are applied.

3.5.3. Effect of coating wettability

Regarding the wettability of the studied samples, Fig. 12 shows that the observed differences in the roughness of the coatings do not entail significant variations in their WCA values. In fact, all the coated samples (except S96p) had similar WCA and W_{adh} values (Table 5) to the uncoated sample (S0p). This fact suggests that the surfaces of the coatings may lead to adhesive forces of a similar magnitude to those of the uncoated sample (S0p). The sample S96p showed the highest WCA (64.4°) and the lowest W_{adh} (104.21 mJ/mm^2), assuming lower adhesive forces than the other samples, and that would have presumably led to weaker bacterial attachment and lower biofilm production. However, the sample S96p showed the highest biofilm production of this study (452%) as well as the highest roughness (105 nm). Therefore, no clear association was identified between the wettability of the analyzed samples and the biofilm production on their surfaces.

Considering all the aforementioned, it can be concluded that higher biofilm production on the coated samples than on the uncoated one is due to an increase in the number *P. aeruginosa* microorganisms adhered to the coatings, as happened in other studies [55,67], which was followed by oxidative stress induction and EPS overproduction. Since the coated samples were generally similar in terms of chemistry and wettability, the increase in their roughness was the main cause of the increased biofilm production.

3.5.4. Bacterial growth

P. aeruginosa growth was determined by measuring the absorbance of the same bacterial inoculum (10^6 cfu/mL) incubated for 0, 3, 6 and 24 h on the uncoated and coated samples. The employed method was based on the measurement of the turbidity of the cellular mass, so as the bacterial concentration increases, the measured absorbance increases. This method does not distinguish between planktonic and sessile bacteria.

Bacterial growth on the uncoated sample (S0p) showed a very similar behavior to that on the coated samples for all the incubation times (Fig. 13). It is worth noting that the sample coated with 12 passes (S12p) is the only one that had more bacterial growth than the S0p sample. On the other hand, in the sample coated with 8 passes (S8p) the bacterial growth was the lowest of all the samples in this study. This lowest bacterial growth in sample S8p is in accordance with the fact that its biofilm production was the lowest of all coated samples (Fig. 8), being even lower than that of sample S4p. The suggested bacterial damage and death that seem to have been caused by the granular pattern of sample S8p with a peak-to-peak distance of 0.83 μm would have resulted in the lowest bacterial growth in the current study, thus producing the lowest amount of biofilm of the coated samples. Nevertheless, more biofilm production was obtained on the coatings than on the uncoated PS while the total amount of bacteria (planktonic and sessile) in the Petri dishes was practically the same for all the studied samples at all times. These results demonstrated that the presence of higher amounts of sessile bacteria on the coated than on the uncoated PS (Fig. 10) was associated to the coating characteristic of promoting the bacterial attachment.

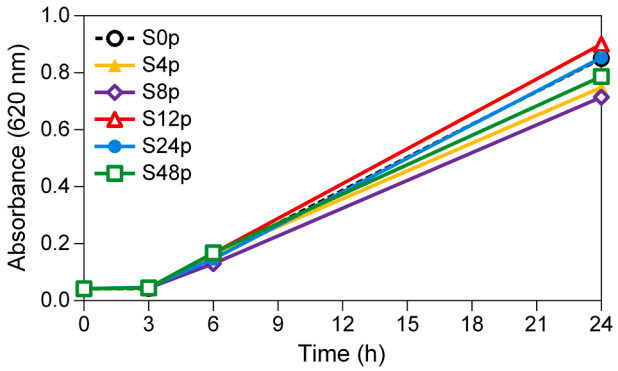

Fig. 13. Bacterial growth after incubation for 0, 3, 6 and 24 h.

3.5.5. Biofilm production speed

The speed of the biofilm production was quantified during 24 h by taking measurements after 6, 12 and 24 h of incubation, and comparing samples S0p and S48p (Fig. 14). The maximum biofilm production measured on sample S48p was produced 6 h after the inoculation, being significantly higher than the biofilm produced on the uncoated sample (S0p) at the same time.

3.6. Proposed pro-biofilm mechanism

The use of APTES as the precursor in atmospheric-pressure plasma-polymerization processes has led to the deposition of coatings that, as our results of this work show, promote the formation of *P. aeruginosa* biofilm. According to the analyses that have been performed on coated and uncoated PS samples, the following mechanism leading to the promotion of biofilm formation on the coatings is suggested.

During the first stages of surface colonization, the electrostatic attraction between the bacteria and the amine groups (NH_2) of the coatings promotes the attachment of more bacterial cells than at the surface of the uncoated PS. Subsequently, the oxygenated carbon groups, which are more abundant on the coatings because they are provided by the APTES molecules and the surrounding atmosphere in the plasma-polymerization process, induce an oxidative stress to the attached bacteria that promotes an overproduction of EPS as a

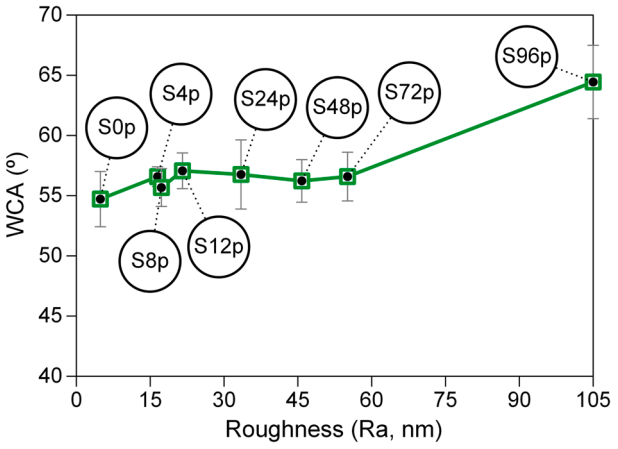

Fig. 12. Relationship between the roughness and the WCA values of the studied samples.

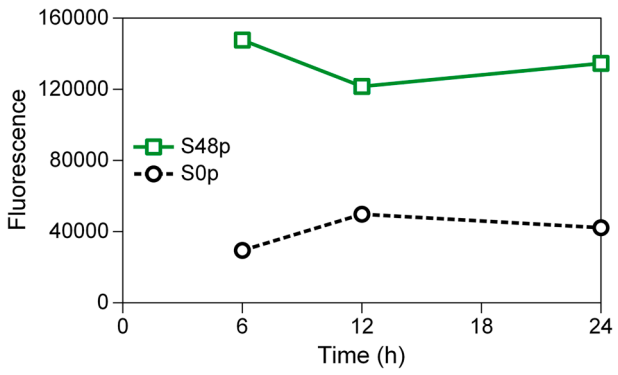

Fig. 14. Biofilm production (measured by FDA method) generated on samples S0p and S48p after incubation for 6, 12 and 24 h.

protective response. Furthermore, once the bacteria are attached to the surface of the coatings, biofilm production is also influenced by the surface topography and roughness. As the number of plasma-polymerization passes increases, the roughness and the biofilm production increase. The increase in the roughness of the coatings is promoted by the deposition of silicon oxide particles. These particles tend to accumulate on the surface features of the PS substrate and give rise to granules that become greater as the number of passes increases. The obtained granular pattern facilitates the formation of bacterial colonies by accumulation and attachment of bacterial cells in its valleys, thus leading to the higher biofilm production as the size of the granules and the roughness increase.

4. Conclusions

The non-thermal plasma jet operating at atmospheric pressure has been revealed as a promising candidate for the preparation of pro-biofilm coatings based on the deposition of siloxane precursor APTES on PS Petri dishes.

The chemical and morphological characteristics of the coatings promoted the higher *P. aeruginosa* biofilm production on their surfaces than on the uncoated PS one. On the one hand, the amine and oxygenated carbon groups that were provided by the APTES molecules promoted the attachment of more bacterial cells and the overproduction of EPS, respectively. Furthermore, the deposition of silicon oxide-based particles gave rise to a granular topographical pattern that increased the roughness of the surface and facilitated the accumulation of bacterial cells in the valleys between granules.

Comparing the coatings, their different biofilm productions were mainly influenced by their roughness, which was directly related to the number of plasma-polymerization passes. Therefore, the higher the number of passes was, the higher the roughness and the biofilm production were. Regarding the chemistry and wettability, no significant enough differences were observed among the different coatings to identify any clear relationship between these characteristics and the different biofilm productions.

Although biofilm in this work was quantified on all the studied samples after 24-h incubation for the sake of a more efficient data management, obtaining a maximum biofilm production after 6-h incubation, as observed on sample S48p, would be of vital importance in real applications (e.g., when proper antibiotic treatment and dose for a patient with a specific infection have to be urgently determined).

It is believed that these findings represent a significant step forward within the fields of disinfectants and antibiotics, and shows promising as a system for testing doses in a simple and fast way.

Considering the identified direct relationship between the coating roughness and the biofilm production, future work will focus on the development of a model that enables the determination of the specific roughness required for the production of a desired amount of biofilm. Also, in order to accelerate the preparation of the surfaces for antibiotic testing as much as possible, biofilm formation for incubation times shorter than 24 h will be more thoroughly studied.

CRediT authorship contribution statement

Elisa Sainz-García: Conceptualization, Methodology, Validation, Formal analysis, Investigation, Data curation, Writing – original draft, Writing – review & editing, Visualization. **María López:** Conceptualization, Methodology, Validation, Formal analysis, Investigation, Data curation, Writing – original draft, Writing – review & editing, Visualization. **Rodolfo Múgica-Vidal:** Conceptualization, Methodology, Validation, Formal analysis, Investigation, Data curation, Writing – review & editing, Visualization, Supervision. **Beatriz Rojo–Bezares:** Conceptualization, Methodology, Formal analysis, Investigation, Data curation, Writing – review & editing. **Carmen Lozano:** Conceptualization, Methodology, Formal analysis, Investigation, Data curation, Writing – review & editing. **Ana González-Marcos:** Conceptualization, Methodology, Formal analysis, Investigation, Data curation, Writing – review & editing. **Paula Toledano:** Conceptualization, Methodology, Formal analysis, Investigation, Data curation, Writing – review & editing. **Ignacio Muro-Fraguas:** Conceptualization, Methodology, Formal analysis, Investigation, Data curation, Writing – review & editing. **Ana Sainz-García:** Conceptualization, Methodology, Formal analysis, Investigation, Data curation, Writing – review & editing. **Yolanda Sáenz:** Conceptualization, Methodology, Formal analysis, Investigation, Resources, Data curation, Writing – review & editing, Visualization, Supervision, Project administration, Funding acquisition. **Fernando Alba-Elías:** Conceptualization, Methodology, Formal analysis, Investigation, Resources, Data curation, Writing – review & editing, Visualization, Supervision, Project administration, Funding acquisition.

Declaration of Competing Interest

The authors declare that they have no known competing financial interests or personal relationships that could have appeared to influence the work reported in this paper.

Acknowledgments

This work was funded by the Programa Estatal de Investigación, Desarrollo e Innovación Orientada a los Retos de la Sociedad through projects AGL2017-82779-C2-1-R and PID2020-113658RB-C21 / AEI / 10.13039/501100011033, and by the Economic Development Agency for La Rioja through project ADER 2019-I-IDD-00074 with co-funding from the European Regional Development Fund (ERDF). The AFM images were taken by the Central Research Support Service (SCAI) of the University of Málaga (UMA). The SEM images of the biofilm on the studied samples were taken by the New Food Preservation and Food Safety Technologies (NEWTEC) research group of the University of León. XPS tests were conducted by the "Advanced Microscopy Laboratory (LMA)" of "The Institute of Nanoscience of Aragon (INA) - University of Zaragoza". The authors would like to thank LMA-INA for access to their equipment and their expertise. The author E. Sainz-García, as post-doctoral researcher of the University of La Rioja, thanks the post-doctoral training program that is funded by the Plan Propio of the University of La Rioja. The authors I. Muro-Fraguas and A. Sainz-García are thankful to the program of pre-doctoral contracts for the training of research staff that is funded by the University of La Rioja.

References

[1] D. Dufour, V. Leung, C.M. Lévesque, Bacterial biofilm: structure, function, and antimicrobial resistance, Endod. Top. 22 (1) (2010) 2–16, https://doi.org/10.1111/j.1601-1546.2012.00277.x.
[2] I.B. Beech, J.A. Sunner, K. Hiraoka, Microbe-surface interactions in biofouling and biocorrosion processes, Int. Microbiol. 8 (2005) 157–168.
[3] A.C. Lee Wong, Biofilms in food processing environments, J. Dairy Sci. 81 (10) (1998) 2765–2770.
[4] C.R. Arciola, D. Campoccia, L. Montanaro, Implant infections: adhesion, biofilm formation and immune evasion, Nat. Rev. Microbiol. 16 (7) (2018) 397–409, https://doi.org/10.1038/s41579-018-0019-y.
[5] M. Magana, C. Sereti, A. Ioannidis, C.A. Mitchell, A.R. Ball, E. Magiorkinis, S. Chatzipanagiotou, M.R. Hamblin, M. Hadjifrangiskou, G.P. Tegos, Options and limitations in clinical investigation of bacterial biofilms, Clin. Microbiol. Rev. 31 (2018) e00084–e116, https://doi.org/10.1128/cmr.00084-16.
[6] N. Høiby, T. Bjarnsholt, M. Givskov, S. Molin, O. Ciofu, Antibiotic resistance of bacterial biofilms, Int. J. Antimicrob. Agents. 35 (4) (2010) 322–332, https://doi.org/10.1016/j.ijantimicag.2009.12.011.
[7] A. Kumar, A. Alam, M. Rani, N.Z. Ehtesham, S.E. Hasnain, Biofilms: Survival and defense strategy for pathogens, Int. J. Med. Microbiol. 307 (8) (2017) 481–489, https://doi.org/10.1016/j.ijmm.2017.09.016.
[8] A. Francesko, M.M. Fernandes, K. Ivanova, S. Amorim, R.L. Reis, I. Pashkuleva, E. Mendoza, A. Pfeifer, T. Heinze, T. Tzanov, Bacteria-responsive multilayer coatings comprising polycationic nanospheres for bacteria biofilm prevention on urinary catheters, Acta Biomater. 33 (2016) 203–212, https://doi.org/10.1016/j.actbio.2016.01.020.

[9] D. Wang, M. Haapasalo, Y. Gao, J. Ma, Y.a. Shen, Antibiofilm peptides against biofilms on titanium and hydroxyapatite surfaces, Bioact. Mater. 3 (4) (2018) 418–425, https://doi.org/10.1016/j.bioactmat.2018.06.002.
[10] V. Prabhawathi, T. Boobalan, P.M. Sivakumar, M. Doble, Functionalized polycaprolactam as an active food package for antibiofilm activity and extended shelf life, Colloids Surfaces B Biointerfaces. 123 (2014) 461–468, https://doi.org/10.1016/j.colsurfb.2014.09.041.
[11] Y. Wu, Y. Ying, Y. Liu, H. Zhang, J. Huang, Preparation of chitosan/poly vinyl alcohol films and their inhibition of biofilm formation against *Pseudomonas aeruginosa* PAO1, Int. J. Biol. Macromol. 118 (2018) 2131–2137, https://doi.org/10.1016/j.ijbiomac.2018.07.061.
[12] Y. Wang, G. Jayan, D. Patwardhan, K.S. Phillips, Antimicrobial and anti-biofilm medical devices: Public health and regulatory science challenges, in: Z. Zhang, V.E. Wagner (Eds.), Antimicrob. Coatings Modif. Med. Devices, Springer International Publishing, 2017: pp. 37–65. doi:10.1007/978-3-319-57494-3.
[13] J. Ivanovic, D. Misic, I. Zizovic, M. Ristic, *In vitro* control of multiplication of some food-associated bacteria by thyme, rosemary and sage isolates, Food Control. 25 (2012) 110–116, https://doi.org/10.1016/j.foodcont.2011.10.019.
[14] L.R. Mulcahy, V.M. Isabella, K. Lewis, *Pseudomonas aeruginosa* biofilms in disease, Microb. Ecol. 68 (1) (2014) 1–12, https://doi.org/10.1007/s00248-013-0297-x.
[15] M.T.T. Thi, D. Wibowo, B.H.A. Rehm, *Pseudomonas aeruginosa* biofilms, Int. J. Mol. Sci. 21 (2020) 8671, https://doi.org/10.3390/ijms21228671.
[16] Z.A. Ali, W.A. Ismail, C.-F. Le, H.M. Jindal, R. Yahya, S. Devi Sekaran, R. Puteh, Antibacterial coating for elimination of *Pseudomonas aeruginosa* and *Escherichia coli*, J. Nanomater. 2014 (2014) 1–6, https://doi.org/10.1155/2014/523530.
[17] H. Ren, J. Wu, A. Colletta, M.E. Meyerhoff, C. Xi, Efficient eradication of mature *Pseudomonas aeruginosa* biofilm via controlled delivery of nitric oxide combined with antimicrobial peptide and antibiotics, Front. Microbiol. 7 (2016) 1260, https://doi.org/10.3389/fmicb.2016.01260.
[18] B.H. Neufeld, M.J. Neufeld, A. Lutzke, S.M. Schweickart, M.M. Reynolds, Metal–organic framework material inhibits biofilm formation of *Pseudomonas aeruginosa*, Adv. Funct. Mater. 27 (34) (2017) 1702255, https://doi.org/10.1002/adfm.201702255.
[19] H. Huang, C. Peng, P. Peng, Y. Lin, X. Zhang, H. Ren, Towards the biofilm characterization and regulation in biological wastewater treatment, Appl. Microbiol. Biotechnol. 103 (3) (2019) 1115–1129, https://doi.org/10.1007/s00253-018-9511-6.
[20] C. Lozano, M. López, B. Rojo-Bezares, Y. Sáenz, Antimicrobial susceptibility testing in *Pseudomonas aeruginosa* biofilms: One step closer to a standardized method, Antibiotics. 9 (2020) 880, https://doi.org/10.3390/antibiotics9120880.
[21] M.D. Macia, E. Rojo-Molinero, A. Oliver, Antimicrobial susceptibility testing in biofilm-growing bacteria, Clin. Microbiol. Infect. 20 (10) (2014) 981–990, https://doi.org/10.1111/1469-0691.12651.
[22] C.A. Nkemngong, M.G. Voorn, X. Li, P.J. Teska, H.F. Oliver, A rapid model for developing dry surface biofilms of *Staphylococcus aureus* and *Pseudomonas aeruginosa* for in vitro disinfectant efficacy testing, Antimicrob. Resist. Infect. Control. 9 (2020) 134, https://doi.org/10.1186/s13756-020-00792-9.
[23] E. Pericolini, B. Colombari, G. Ferretti, R. Iseppi, A. Ardizzoni, M. Girardis, A. Sala, S. Peppoloni, E. Blasi, Real-time monitoring of *Pseudomonas aeruginosa* biofilm formation on endotracheal tubes in vitro, BMC Microbiol. 18 (2018) 84, https://doi.org/10.1186/s12866-018-1224-6.
[24] E. Ning, G. Turnbull, J. Clarke, F. Picard, P. Riches, M. Vendrell, D. Graham, A. W. Wark, K. Faulds, W. Shu, 3D bioprinting of mature bacterial biofilms for antimicrobial resistance drug testing, Biofabrication. 11 (4) (2019) 045018, https://doi.org/10.1088/1758-5090/ab37a0.
[25] N.E. Harrington, E. Sweeney, F. Harrison, Building a better biofilm - Formation of *in vivo*-like biofilm structures by *Pseudomonas aeruginosa* in a porcine model of cystic fibrosis lung infection, Biofilm. 2 (2020) 100024, https://doi.org/10.1016/j.bioflm.2020.100024.
[26] M. Hernández-Orta, E. Pérez, L.E. Cruz-Barba, M.A. Sánchez-Castillo, Synthesis of bactericidal polymer coatings by sequential plasma-induced polymerization of 4-vinyl pyridine and gas-phase quaternization of poly-4-vinyl pyridine, J. Mater. Sci. 53 (12) (2018) 8766–8785, https://doi.org/10.1007/s10853-018-2183-x.
[27] K.J. Brobbey, J. Haapanen, J.M. Mäkelä, M. Gunell, E. Eerola, E. Rosqvist, J. Peltonen, J.J. Saarinen, M. Tuominen, M. Toivakka, Effect of plasma coating on antibacterial activity of silver nanoparticles, Thin Solid Films. 672 (2019) 75–82, https://doi.org/10.1016/j.tsf.2018.12.049.
[28] D.S. Trentin, F. Bonatto, K.R. Zimmer, V.B. Ribeiro, A.L.S. Antunes, A.L. Barth, G. V. Soares, C. Krug, I.J.R. Baumvol, A.J. Macedo, N_2/H_2 plasma surface modifications of polystyrene inhibit the adhesion of multidrug resistant bacteria, Surf. Coatings Technol. 245 (2014) 84–91, https://doi.org/10.1016/j.surfcoat.2014.02.046.
[29] C. Pignata, D. D'Angelo, E. Fea, G. Gilli, A review on microbiological decontamination of fresh produce with nonthermal plasma, J. Appl. Microbiol. 122 (6) (2017) 1438–1455, https://doi.org/10.1111/jam.13412.
[30] P. Puligundla, T. Lee, C. Mok, Inactivation effect of dielectric barrier discharge plasma against foodborne pathogens on the surfaces of different packaging materials, Innov. Food Sci. Emerg. Technol. 36 (2016) 221–227, https://doi.org/10.1016/j.ifset.2016.06.027.
[31] R. Bitar, P. Cools, N. De Geyter, R. Morent, Acrylic acid plasma polymerization for biomedical use, Appl. Surf. Sci. 448 (2018) 168–185, https://doi.org/10.1016/j.apsusc.2018.04.129.
[32] M.C. Ramkumar, K. Navaneetha Pandiyaraj, A. Arun Kumar, P.V.A. Padmanabhan, P. Cools, N. De Geyter, R. Morent, S. Uday Kumar, V. Kumar, P. Gopinath, S. K. Jaganathan, R.R. Deshmukh, Atmospheric pressure non-thermal plasma assisted polymerization of poly (ethylene glycol) methylether methacrylate (PEGMA) on low density polyethylene (LDPE) films for enhancement of biocompatibility, Surf. Coatings Technol. 329 (2017) 55–67, https://doi.org/10.1016/j.surfcoat.2017.09.020.
[33] E. Sardella, F. Palumbo, G. Camporeale, P. Favia, Non-equilibrium plasma processing for the preparation of antibacterial surfaces, Materials (Basel). 9 (2016) 515, https://doi.org/10.3390/ma9070515.
[34] M. Cloutier, D. Mantovani, F. Rosei, Antibacterial coatings: Challenges, perspectives, and opportunities, Trends Biotechnol. 33 (11) (2015) 637–652, https://doi.org/10.1016/j.tibtech.2015.09.002.
[35] A. Nikiforov, X. Deng, Q. Xiong, U. Cvelbar, N. DeGeyter, R. Morent, C. Leys, Non-thermal plasma technology for the development of antimicrobial surfaces: a review, J. Phys. D. Appl. Phys. 49 (20) (2016) 204002, https://doi.org/10.1088/0022-3727/49/20/204002.
[36] K. Vasilev, M. Ramiasa-MacGregor, Nanoengineered plasma polymer films for biomedical applications, Adv. Mater. Lett. 9 (1) (2018) 42–52, https://doi.org/10.5185/amlett.2018.1691.
[37] E. Sainz-García, F. Alba-Elías, R. Múgica-Vidal, A. González-Marcos, Enhanced surface friction coefficient and hydrophobicity of TPE substrates using an APPJ system, Appl. Surf. Sci. 328 (2015) 554–567, https://doi.org/10.1016/j.apsusc.2014.12.084.
[38] J.F. Moulder, W.F. Stickle, P.E. Sobol, K.D. Bomben, Handbook of X-Ray Photoelectron Spectroscopy, Perkin-Elmer Corporation, Eden Prairie, Minnesota (1992), https://doi.org/10.1002/sia.740030412.
[39] C.A. Schneider, W.S. Rasband, K.W. Eliceiri, NIH Image to ImageJ: 25 years of image analysis, Nat. Methods. 9 (7) (2012) 671–675, https://doi.org/10.1038/nmeth.2089.
[40] A.F. Stalder, T. Melchior, M. Müller, D. Sage, T. Blu, M. Unser, Low-bond axisymmetric drop shape analysis for surface tension and contact angle measurements of sessile drops, Colloids Surf. A Physicochem. Eng. Asp. 364 (1-3) (2010) 72–81, https://doi.org/10.1016/j.colsurfa.2010.04.040.
[41] R.R. Deshmukh, A.R. Shetty, Comparison of surface energies using various approaches and their suitability, J. Appl. Polym. Sci. 107 (6) (2008) 3707–3717, https://doi.org/10.1002/app.27446.
[42] E. Peeters, H.J. Nelis, T. Coenye, Comparison of multiple methods for quantification of microbial biofilms grown in microtiter plates, J. Microbiol. Methods. 72 (2) (2008) 157–165, https://doi.org/10.1016/j.mimet.2007.11.010.
[43] M. Mokter Hossain, Q.H. Trinh, M.S.P. Sudhakaran, L. Sultana, Y.S. Mok, Improvement of mechanical strength of hydrophobic coating on glass surfaces by an atmospheric pressure plasma jet, Surf. Coatings Technol. 357 (2019) 12–22, https://doi.org/10.1016/j.surfcoat.2018.09.071.
[44] E. Sainz-García, F. Alba-Elías, R. Múgica-Vidal, A. González-Marcos, Antifriction aminopropyltriethoxysilane films on thermoplastic elastomer substrates using an APPJ system, Surf. Coatings Technol. 310 (2017) 239–250, https://doi.org/10.1016/j.surfcoat.2016.12.079.
[45] A. Soum-Glaude, L. Thomas, E. Tomasella, Amorphous silicon carbide coatings grown by low frequency PACVD: Structural and mechanical description, Surf. Coatings Technol. 200 (22-23) (2006) 6425–6429, https://doi.org/10.1016/j.surfcoat.2005.11.066.
[46] B. Borer, SiO_x Thin Film Deposition on Particles by Plasma Enhanced Chemical Vapor Deposition in a Circulating Fluidized Bed Reactor, Swiss Federal Institute of Technology Zurich (2005). http://e-collection.library.ethz.ch/eserv/eth:28482/eth-28482-02.pdf.
[47] B. Borer, A. Sonnenfeld, P.h. Rudolf von Rohr, Influence of substrate temperature on morphology of SiO_x films deposited on particles by PECVD, Surf. Coatings Technol. 201 (3-4) (2006) 1757–1762, https://doi.org/10.1016/j.surfcoat.2006.03.001.
[48] E.H. Lock, D.Y. Petrovykh, P. Mack, T. Carney, R.G. White, S.G. Walton, R. F. Fernsler, Surface composition, chemistry, and structure of polystyrene modified by electron-beam-generated plasma, Langmuir. 26 (11) (2010) 8857–8868, https://doi.org/10.1021/la9046337.
[49] S.R. Kane, P.D. Ashby, L.A. Pruitt, ATR-FTIR as a thickness measurement technique for hydrated polymer-on-polymer coatings, J. Biomed. Mater. Res. - Part B Appl. Biomater. 91B (2) (2009) 613–620, https://doi.org/10.1002/jbm.b.31436.
[50] O.M. Ba, P. Marmey, K. Anselme, A.C. Duncan, A. Ponche, Surface composition XPS analysis of a plasma treated polystyrene: Evolution over long storage periods, Colloids Surf. B Biointerfaces. 145 (2016) 1–7, https://doi.org/10.1016/j.colsurfb.2016.04.026.
[51] E. Sainz-García, F. Alba-Elías, R. Múgica-Vidal, M. Pantoja-Ruiz, Promotion of tribological and hydrophobic properties of a coating on TPE substrates by atmospheric plasma-polymerization, Appl. Surf. Sci. 371 (2016) 50–60, https://doi.org/10.1016/j.apsusc.2016.02.186.
[52] A. Manakhov, J. Čechal, M. Michlíček, D.V. Shtansky, Determination of NH_2 concentration on 3-aminopropyl tri-ethoxy silane layers and cyclopropylamine plasma polymers by liquid-phase derivatization with 5-iodo 2-furaldehyde, Appl. Surf. Sci. 414 (2017) 390–397, https://doi.org/10.1016/j.apsusc.2017.04.127.
[53] S. Ben Said, F. Arefi-Khonsari, J. Pulpytel, Plasma polymerization of 3-aminopropyltrietoxysilane (APTES) by open-air atmospheric arc plasma jet for in-line treatments, Plasma Process. Polym. 13 (10) (2016) 1025–1035, https://doi.org/10.1002/ppap.201600079.
[54] S. Das, S. Singh, V. Singh, D. Joung, J.M. Dowding, D. Reid, J. Anderson, L. Zhai, S. I. Khondaker, W.T. Self, S. Seal, Oxygenated functional group density on graphene oxide: Its effect on cell toxicity, Part. Part. Syst. Charact. 30 (2) (2013) 148–157, https://doi.org/10.1002/ppsc.201200066.
[55] S. Gao, X. Dong, J. Huang, S. Li, Y. Li, Z. Chen, Y. Lai, Rational construction of highly transparent superhydrophobic coatings based on a non-particle, fluorine-

free and water-rich system for versatile oil-water separation, Chem. Eng. J. 333 (2018) 621–629, https://doi.org/10.1016/j.cej.2017.10.006.
[56] M. Kargar, Y.-R. Chang, H. Khalili Hoseinabad, A. Pruden, W.A. Ducker, Colloidal crystals delay formation of early stage bacterial biofilms, ACS Biomater. Sci. Eng. 2 (6) (2016) 1039–1048, https://doi.org/10.1021/acsbiomaterials.6b00163.
[57] S.M. Kelleher, O. Habimana, J. Lawler, B. O' Reilly, S. Daniels, E. Casey, A. Cowley, Cicada wing surface topography: An investigation into the bactericidal properties of nanostructural features, ACS Appl. Mater. Interfaces. 8 (24) (2016) 14966–14974, https://doi.org/10.1021/acsami.5b08309.
[58] E. Preedy, S. Perni, D. Nipiĉ, K. Bohinc, P. Prokopovich, Surface roughness mediated adhesion forces between borosilicate glass and gram-positive bacteria, Langmuir. 30 (31) (2014) 9466–9476, https://doi.org/10.1021/la501711t.
[59] D. Perera-Costa, J.M. Bruque, M.L. González-Martín, A.C. Gómez-García, V. Vadillo-Rodríguez, Studying the influence of surface topography on bacterial adhesion using spatially organized microtopographic surface patterns, Langmuir. 30 (16) (2014) 4633–4641, https://doi.org/10.1021/la5001057.
[60] M. Abrigo, P. Kingshott, S.L. McArthur, Electrospun polystyrene fiber diameter influencing bacterial attachment, proliferation, and growth, ACS Appl. Mater. Interfaces. 7 (14) (2015) 7644–7652, https://doi.org/10.1021/acsami.5b00453.
[61] Y. Yuan, M.P. Hays, P.R. Hardwidge, J. Kim, Surface characteristics influencing bacterial adhesion to polymeric substrates, RSC Adv. 7 (23) (2017) 14254–14261.
[62] M. Lorenzetti, I. Dogša, T. Stošicki, D. Stopar, M. Kalin, S. Kobe, S. Novak, The influence of surface modification on bacterial adhesion to titanium-based substrates, ACS Appl. Mater. Interfaces. 7 (3) (2015) 1644–1651, https://doi.org/10.1021/am507148n.
[63] E. Medilanski, K. Kaufmann, L.Y. Wick, O. Wanner, H. Harms, Influence of the surface topography of stainless steel on bacterial adhesion, Biofouling. 18 (3) (2002) 193–203, https://doi.org/10.1080/08927010290011370.
[64] S. Wu, B. Zhang, Y. Liu, X. Suo, H. Li, Influence of surface topography on bacterial adhesion: A review, Biointerphases. 13 (2018), 060801, https://doi.org/10.1116/1.5054057.
[65] A. Tripathy, P. Sen, B. Su, W.H. Briscoe, Natural and bioinspired nanostructured bactericidal surfaces, Adv. Colloid Interface Sci. 248 (2017) 85–104, https://doi.org/10.1016/j.cis.2017.07.030.
[66] S. Wu, S. Altenried, A. Zogg, F. Zuber, K. Maniura-Weber, Q. Ren, Role of the surface nanoscale roughness of stainless steel on bacterial adhesion and microcolony formation, ACS Omega. 3 (6) (2018) 6456–6464, https://doi.org/10.1021/acsomega.8b00769.
[67] Method for forming biofilm and biofilm fixing material, JP2013173715, 2013.
[68] M.E. Villanueva, A. Salinas, G.J. Copello, L.E. Díaz, Point of zero charge as a factor to control biofilm formation of *Pseudomonas aeruginosa* in sol-gel derivatized aluminum alloy plates, Surf. Coat. Technol. 254 (2014) 145–150, https://doi.org/10.1016/j.surfcoat.2014.05.074.
[69] K. Mathee, O. Ciofu, C. Sternberg, P.W. Lindum, J.I.A. Campbell, P. Jensen, A. H. Johnsen, M. Givskov, D.E. Ohman, S. Molin, N. Høiby, A. Kharazmi, Mucoid conversion of *Pseudomonas aeruginosa* by hydrogen peroxide: a mechanism for virulence activation in the cystic fibrosis lung, Microbiology. 145 (1999) 1349–1357.
[70] M. Hentzer, G.M. Teitzel, G.J. Balzer, A. Heydorn, S. Molin, M. Givskov, M. R. Parsek, Alginate overproduction affects *Pseudomonas aeruginosa* biofilm structure and function, J. Bacteriol. 183 (18) (2001) 5395–5401, https://doi.org/10.1128/JB.183.18.5395-5401.2001.